Journal of Water & Health

© 2023 The Authors

Journal of Water and Health Vol 21 No 7, 869 doi: 10.2166/wh.2023.025

# Enhancement of adsorptive removal efficiency of an anionic dye from aqueous solutions using carboxylic acid-modified mulberry leaves: Artificial neural network modeling, isotherm, and kinetics evaluation

Celal Duran [a,*], Sengul Tugba Ozeken[a], Aslihan Yilmaz Camoglu[a] and Duygu Ozdes[b]

[a] Faculty of Sciences, Department of Chemistry, Karadeniz Technical University, 61080 Trabzon, Türkiye
[b] Gumushane Vocational School, Chemistry and Chemical Processing Technologies Department, Gumushane University, 29100 Gumushane, Türkiye
*Corresponding author. E-mail: cduran@ktu.edu.tr

CD, 0000-0002-1306-9061

## ABSTRACT

Natural mulberry leaves and carboxylic acid-modified mulberry (*Morus alba* L.) leaves were used for the first time to scrutinize the effects of modification on the retention efficiency of an anionic dye (Remazol Brilliant Blue R (RBBR)) from aqueous solutions to suggest an economical and promising adsorbent for the treatment of dye-contaminated water. The characterization of the adsorbents was accomplished through common techniques including SEM, FTIR, and $pH_{pzc}$ determination. Several parameters studied in batch experiments pointed out that the initial pH of 2.0 and the contact time of 240 min were optimum conditions for all the developed RBBR uptake processes. An artificial neural network (ANN) model was applied to formulate a forecast model for the uptake efficiency of RBBR. The experimental data were assessed by different kinetic and isotherm models to explain the mechanism of the developed processes in more detail. Maximum monolayer adsorption capacities of natural mulberry leaves and acetic acid-, citric acid-, and oxalic acid-modified mulberry leaves were determined as 64.5, 95.2, 84.8, and 91.7 mg $g^{-1}$, respectively, by the Langmuir isotherm model. These results demonstrated that the modification with carboxylic acids significantly increases the anionic dye adsorption capacity of the mulberry leaves.

**Key words:** adsorption, artificial neural network, isotherm, kinetics, mulberry leaves, Remazol brilliant blue R

## HIGHLIGHTS

- Natural mulberry leaves and carboxylic acid-modified mulberry leaves were used for the adsorptive removal of an anionic dye for the first time.
- An economical and promising adsorbent was developed for industrial wastewater treatment applications.
- Modification with carboxylic acids significantly increases the anionic dye adsorption capacity of the mulberry leaves.
- ANN model is suitable for the prediction of RBBR adsorption efficiency.

This is an Open Access article distributed under the terms of the Creative Commons Attribution Licence (CC BY 4.0), which permits copying, adaptation and redistribution, provided the original work is properly cited (http://creativecommons.org/licenses/by/4.0/).

Downloaded from http://iwaponline.com/jwh/article-pdf/21/7/869/1263352/jwh0210869.pdf
by guest

## GRAPHICAL ABSTRACT

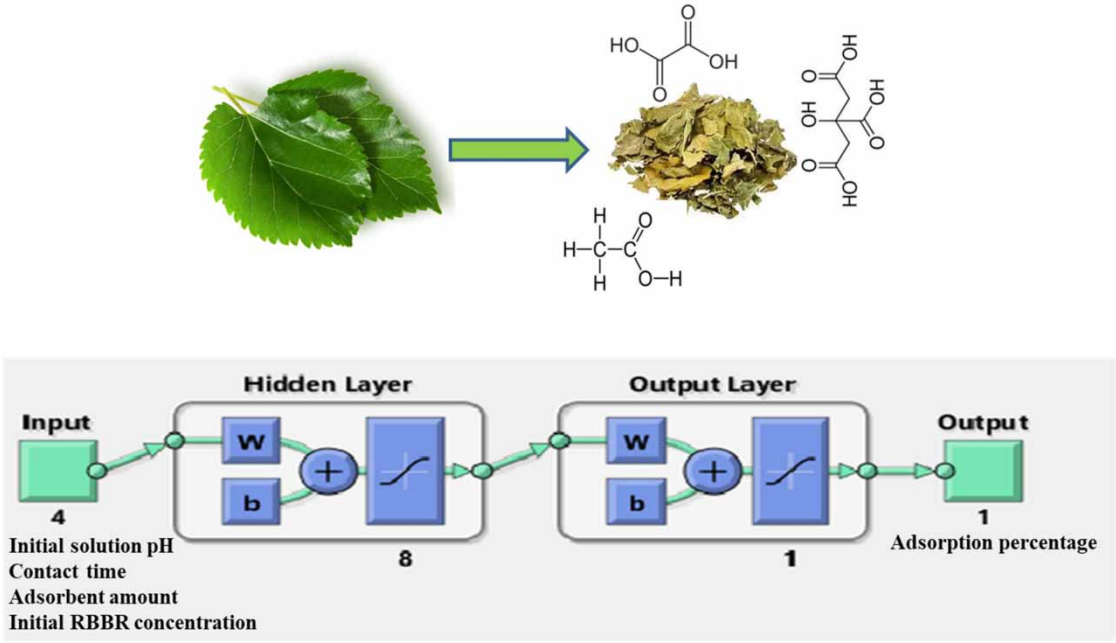


## 1. INTRODUCTION

The employment of dyes in industrial branches has become quite popular with the development of industry and technology. However, the production of new dyestuffs and detailing of the color scale actually increased the rate of the usage of synthetic dyes that are harmful to nature. Synthetic dyes that are extremely resistant to biodegradation by microorganisms are commonly employed for product coloration in paper, textile, tanning, leather, plastic, rubber, pharmaceutical, food, and cosmetic industries (Vijayaraghavan & Yun 2008; Ali 2010; Ahmad *et al.* 2014). Considering the volume and composition of discharged wastewater, the textile industry has become the most polluting industrial sector for the environment and represents a challenge to conventional biological, physical, or chemical treatment methods (Wang *et al.* 2006). The release of synthetic dye-contaminated industrial wastewater into surface waters induces serious irreversible damage to both living organisms and the environment (Shojaei *et al.* 2021).

Remazol brilliant blue R (RBBR), an anionic dye derived from anthraquinone, is extensively employed in several industrial activities, especially in the production of polymeric dye, and it causes harmful effects on human metabolism by reaching both aquatic organisms and the food chain even at trace amounts (Mechichi *et al.* 2006). Removal of RBBR and other hazardous dyes from industrial wastewater – before discharging step – is essential for the safety of the environment and all living organisms. There are several physical, chemical, or biological methods, including adsorption, sedimentation, floatation, flocculation, coagulation, reverse osmosis/ultrafiltration, electrolysis, ion exchange, ozonation, and anaerobic digestion for dye-contaminated wastewater treatment (Ewuzie *et al.* 2022). Among numerous methods, adsorption has attracted attention due to its fast application, low cost, efficiency, environmental friendliness, as well as its applicability in the treatment of synthetic dyes from large volumes of wastewater generated from worldwide industrial applications (Vakili *et al.* 2014; Liu *et al.* 2018). The efficiency and applicability of the adsorption process depend directly on the properties of the adsorbent used. Numerous agricultural and industrial wastes or some other materials including bagasse fly ash (Chumpiboon *et al.* 2022), shale oil ash (Miyah *et al.* 2021), cellulose-based activated carbon (Zhang *et al.* 2022), almond shell (Ozdes *et al.* 2010; Senturk *et al.* 2010; Duran *et al.* 2011), rice bran-based magnetic composite (Ma *et al.* 2020), metal oxide nanocomposites (Hong & Wang 2017; Reghioua *et al.* 2021), clay (Ozdes *et al.* 2014; Jawad *et al.* 2022), and laccases (Herkommerová *et al.* 2018) have been employed as an adsorbent for the retention of various synthetic dyestuffs.

Mulberry (*Morus alba* L.) can be grown in many regions due to its high adaptability to different soil and climate conditions (Karadeniz & Osma 2019). Both natural and modified mulberry leaves have been applied by previous researchers in the

Downloaded from http://iwaponline.com/jwh/article-pdf/21/7/869/1263352/jwh0210869.pdf
by guest

adsorption of various dyestuffs. Siraorarnroj *et al.* (2022) have prepared nanoporous carbon of the mulberry leaves through hydrothermal-carbonization with microwave processing using a chemical reagent (MPC) for the adsorption of methyl orange (MO). Khan & Farooqui (2022) have employed mulberry leaves biochar for the retention of methylene blue (MB) from aqueous solutions. Modification of adsorbents with chemical substances, especially different types of acids, improves their adsorption capacity and enables more effective adsorbents to be obtained. For this purpose, carboxylic acids are widely applied. Tian *et al.* (2020) have prepared carboxylic acid-modified bamboo powder for Pb(II) ions retention from aqueous media. Nayak & Pal (2021) have modified *Abelmoschus esculentus* seeds with oxalic, citric, and tartaric acids to enhance the adsorption of gentian violet. Guo *et al.* (2022) have used acrylic acid-modified walnut shells for the uptake of Rhodamine B.

The present investigation aims to propose a cost-efficient alternative for the adsorption of RBBR from aqueous media by employing carboxylic acid (acetic acid (AA), citric acid (CA), and oxalic acid (OA))-modified mulberry leaves. According to our literature survey, carboxylic acid-modified mulberry leaves were employed for the first time for the retention of a dyestuff in the present research. There are millions of tons of mulberry leaves as agricultural waste all over the world. Mulberry leaves, which have no usage area and are just thrown away, were reprocessed with outstanding environmental practice in the present study. The application of a three-layer artificial neural network (ANN) model was illustrated to model and predict the adsorption efficiency of RBBR. The independent experimental conditions including solution pH, contact time, adsorbent amount, and initial RBBR concentration were applied as input parameters to train the neural network while adsorption percentage, a dependent variable, was considered as the output layer of the neural network. The best experimental conditions were evaluated and optimized for RBBR retention. In addition, the experimental data were analyzed by different kinetics and isotherm models to evaluate the adsorption mechanism.

## 2. MATERIALS AND METHODS

### 2.1. Reagents and instrumentation

RBBR, which has a chemical formula of $C_{22}H_{16}N_2Na_2O_{11}S_3$, a molar mass of 626.53 g $mol^{-1}$, and a maximum absorbance value of 592 nm, was used as an adsorbate in the present research. All of the chemicals used in the study including RBBR, OA, AA, CA, NaOH, and $HNO_3$ were of analytical purity and obtained from Fluka (Buch, Switzerland) or Merck (Darmstadt, Germany). The working and calibration solutions were obtained by the dilution of the stock RBBR solution, at a concentration of 5,000 mg $L^{-1}$. Distilled water was used in all stages of the experiments. Diluted NaOH and $HNO_3$ solutions were used for adjusting the initial pH of RBBR solutions. All glassware used in the experimental studies was kept in 5% (v/v) $HNO_3$ solution for 12 h, and then washed with tap water and distilled water, respectively. The RBBR concentration in aqueous solution was detected with Perkin Elmer Lambda 25 model UV–Vis spectrophotometer. Hanna pH-2221 model desktop pH meter to adjust the pH values of the solutions, Edmund Bühler GmbH model mechanical shaker for adsorption experiments, and BOECO S-8 model centrifuge apparatus to separate the adsorbent from the solutions were used. Fourier Transform Infrared Spectrometer (Perkin Elmer 1600 Series) was benefitted to illuminate the functional groups of natural and carboxylic acid-modified mulberry leaves while their morphological structure was elucidated by Scanning Electron Microscope (ZIESS Evo Ls 10).

### 2.2. Preparation of the adsorbents

For the adsorption of RBBR from an aqueous solution, mulberry (*M. alba* L.) leaves modified with AA, CA, and OA were used. Mulberry leaves were picked up from the countryside of Gümüşhane, a city in the Blacksea region of Türkiye. The leaves were washed with tap water and distilled water several times to remove any environmental dust and then they were dried in an oven at 80 °C for 24 h. A blender was used to grind the leaves and particles smaller than 150 μm (<150 μm) were used in the modification process. The modification of mulberry leaves with carboxylic acids including AA, CA, and OA was implemented according to Tian *et al.* (2020) with a little change. Briefly, 5.0 g of dried mulberry leaves were mixed with 0.2 M of 100 mL AA, CA, and OA solutions, separately. The stirring of these suspensions was carried out at 120 rpm for 24 h at room temperature. At the end of this process, the mixtures were filtrated through 0.45 μm pore-sized filter paper and the adsorbents on the filter paper were washed with distilled water several times. The modified adsorbents were dried in an oven at 80 °C and then kept in glass bottles until the experimental studies. The natural mulberry leaves and AA-, CA-, and OA-modified mulberry leaves were named NML, AAM, CAM, and OAM, respectively.

Downloaded from http://iwaponline.com/jwh/article-pdf/21/7/869/1263352/jwh0210869.pdf
by guest

### 2.3. Batch adsorption experiments

The batch method was performed to assess the influences of experimental variables such as initial solution pH, equilibrium time, initial RBBR concentration, and adsorbent concentration on the adsorption efficiency of RBBR onto NML, AAM, CAM, and OAM. In a typical procedure, each of the adsorbents was weighed in the range of 10–200 mg, separately in 15 mL of polypropylene centrifuge tubes. Then, 10 mL of RBBR solutions at an initial pH value of 2.0 in the concentration range between 50 and 1,000 mg $L^{-1}$ were added and the mixtures obtained were mixed in a mechanical shaker at 400 rpm in time intervals of 1–480 min. Based on the results of our previous study, a shaking speed of 400 rpm was found to be sufficient for the adsorption (Ozdes *et al.* 2010). Therefore, shaking speed was not optimized in the present study and all of the experiments were carried out at a constant shaking speed. At the end of the determined times, the centrifugation was carried out at 1,180 *g* for 5 min to separate the adsorbent from the solution. The RBBR concentration remaining in the solution was measured with UV–Vis Spectrophotometer at a wavelength of 592 nm. All experiments were performed in triplicate. The amount of RBBR adsorbed by per gram of adsorbent ($q_e$ (mg $g^{-1}$)) was assessed using Equation (1):

$$q_e = \frac{V(Co - Ce)}{m_s} \tag{1}$$

where $C_o$ and $C_e$ are the initial and equilibrium concentrations of RBBR (mg $L^{-1}$), respectively, $V$ is the volume of the aqueous solution (L), and $m_s$ is the dry mass of adsorbent (g) used in the experiment.

### 2.4. ANN modeling

In order to get a prediction model for the adsorption of RBBR onto AAM, CAM, and OAM, artificial neural networks (ANNs) were operated by utilizing the Neural Network Toolbox in MATLAB R2017b mathematical software. ANN involves three main layers as input, hidden, and output layers. In the present research, the solution pH, contact time, adsorbent amount, and initial RBBR concentration were preferred as input parameters and the adsorption percentage was designated as the output parameter. In this regard, a three-layer backpropagation (BP) neural network model with a tangent sigmoid transfer function (tansig) at the hidden layer and a linear transfer function (purelin) at the output layer was practiced. In order to train the network, Levenberg–Marquardt back propagation (LMB) algorithm was performed (Khajeh *et al.* 2015; Ghadirimoghaddam *et al.* 2021). The performance of the network was evaluated by the correlation coefficient ($R^2$) used as a function of the error. The optimum architecture of the ANN model was constructed as 4-8-1 as given in Supplementary material, Figure S1.

## 3. RESULTS AND DISCUSSION

### 3.1. Characterization of the adsorbents

In order to investigate the functional groups on both NBL and carboxylic acid-modified mulberry leaves, the FTIR spectrum of each adsorbent was acquired in the range of 4,000–650 $cm^{-1}$. FTIR spectra of the modified adsorbents were not significantly different from the spectrum of natural adsorbents, revealing that the modification process did not cause any change in the surface functional groups. A band at 3,290 $cm^{-1}$ is associated with –OH groups due to the presence of alcoholic, phenolic, and carboxylic groups. The aliphatic C–H stretching vibration is noticed at 2,920 and 2,850 $cm^{-1}$. The C = C stretching vibration and C = O bond of the carboxylic group are seen at 1,620 and 1,730 $cm^{-1}$, respectively. The C–O stretching vibration is noticed at 1,027.5 $cm^{-1}$ (Malook & Khan 2020) (Figure 1). The surface morphology of NML, AAM, OAM, and CAM was scrutinized by SEM analyses. When SEM structures are examined, it is noticed that NML is more porous than the modified adsorbents. After the modification process, the existing porous structures disappeared significantly and the surface of NML was covered with carboxylic acids (Figure 2). In addition to these, the point of zero charge ($pH_{pzc}$) of NML, AAM, CAM, and OAM was ascertained as 6.0, 5.1, 3.9, and 7.1, respectively.

### 3.2. Influences of initial pH on the adsorption efficiency of RBBR

The initial pH of aqueous solution acts a significant part in the adsorption process since the chemical structure of the adsorbate and the surface charge of the adsorbent are directly affected by the solution pH. Therefore, the uptake efficiency of RBBR on NML, AAM, CAM, and OAM was tested in the initial solution pH range of 2.0–8.0, at initial RBBR concentration of 100 mg $L^{-1}$ by using 5.0 g $L^{-1}$ g of each adsorbent. As the initial solution pH is increased from 2.0 to 8.0, the $q_e$ values appear to decrease from 18.4 to 2.1 mg $g^{-1}$ for NML, from 19.1 to 5.7 mg $g^{-1}$ for AAM, from 19.4 to 7.4 mg $g^{-1}$ for CAM,

Downloaded from http://iwaponline.com/jwh/article-pdf/21/7/869/1263352/jwh0210869.pdf
by guest

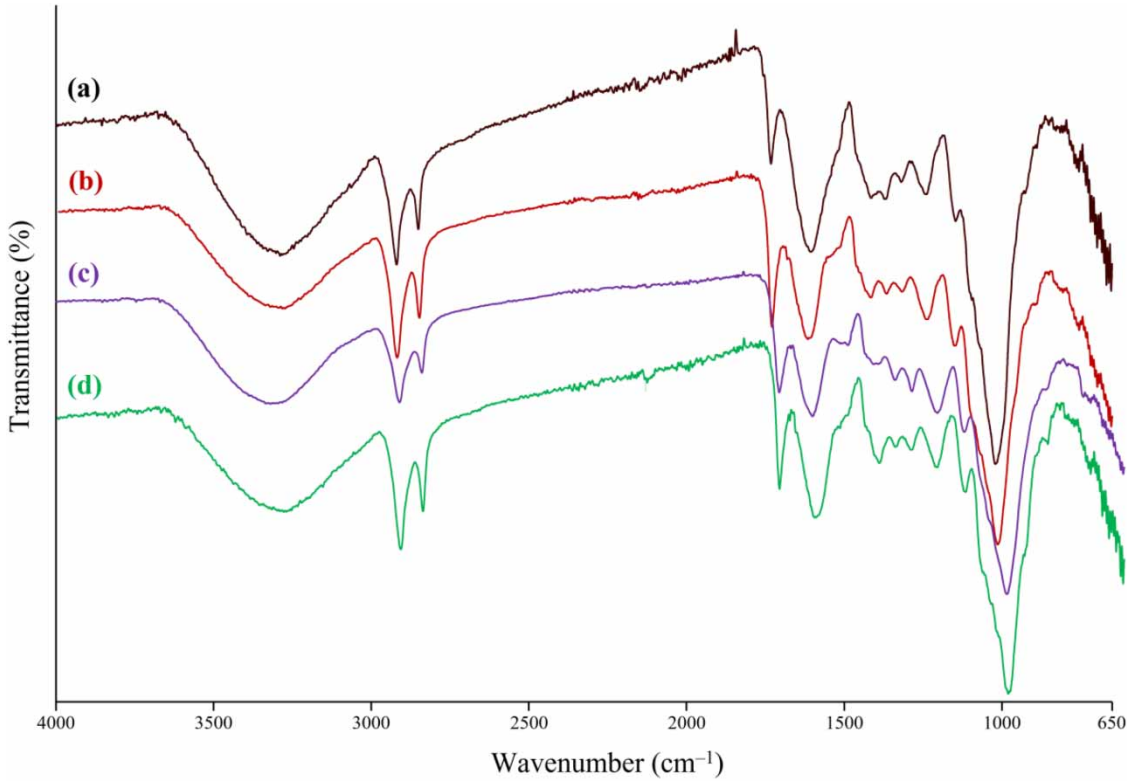


**Figure 1** | FTIR spectrum of (a) natural mulberry leaves (NML); (b) acetic acid-modified mulberry leaves (AAM); (c) citric acid-modified mulberry leaves (CAM); and (d) oxalic acid-modified mulberry leaves (OAM).

and from 19.2 to 6.7 mg g$^{-1}$ for OAM (Figure 3). At low pH values (pH < $pH_{pzc}$), adsorbent surfaces are surrounded by $H_3O^+$ ions, and their surface functional groups are positively charged (–$COOH_2^+$). Therefore, electrostatic interaction occurs between the anionic RBBR molecules and the positively charged adsorbent surfaces, which increases the uptake efficiency. On the contrary, with the increase in the initial solution pH value (pH > $pH_{pzc}$), the negative charge density on the adsorbent's surface ($COO^-$) begins to increase and accordingly, the electrostatic repulsion between RBBR molecules and adsorbent surfaces increases, which decreases the adsorption efficiency (Moharami & Jalali 2013). The $pH_{pzc}$ values of NML, AAM, CAM, and OAM were determined as 6.0, 5.1, 3.9, and 7.1, respectively and it is expected that RBBR, which is an anionic dye, will be removed with the highest efficiency at lower pH values than these values. As a result, further experiments were planned by considering the optimum initial solution pH as 2.0 for all types of adsorbents.

### 3.3. Evaluation of equilibrium time and adsorption kinetics

Removal of hazardous dyes from the wastewater should be economical for real industrial applications, since large amounts of industrial wastewater are being discharged into the environment. Therefore, it is critical to ascertain the minimum time at which maximum dye retention occurs. In order to evaluate the optimum equilibrium time for RBBR adsorption; 0.05 g (5.0 g L$^{-1}$) of AAM, CAM, and OAM were treated separately with 100 mg L$^{-1}$ of RBBR solution at different contact times in the range of 1–480 min. On completion of each specified period, the adsorbents were separated from the solution through centrifugation and the levels of unadsorbed RBBR in the solution were determined by UV–Vis Spectrophotometer. The RBBR amounts ($q_t$) adsorbed by 1 g of AAM, CAM, and OAM at different time intervals were calculated. In the initial steps of the adsorption process, the adsorption occurred rapidly due to the open adsorption sites on the surface of the adsorbents. Over time, the uptake rate of RBBR decreased as the adsorbent pores were filled, and after 240 min of contact time, the equilibrium was achieved due to the complete saturation of the adsorbent surface. As a result, the sufficient time for the adsorption of RBBR onto all adsorbent surfaces was determined as 240 min for subsequent studies (Supplementary material, Figure S2).

Downloaded from http://iwaponline.com/jwh/article-pdf/21/7/869/1263352/jwh0210869.pdf
by guest

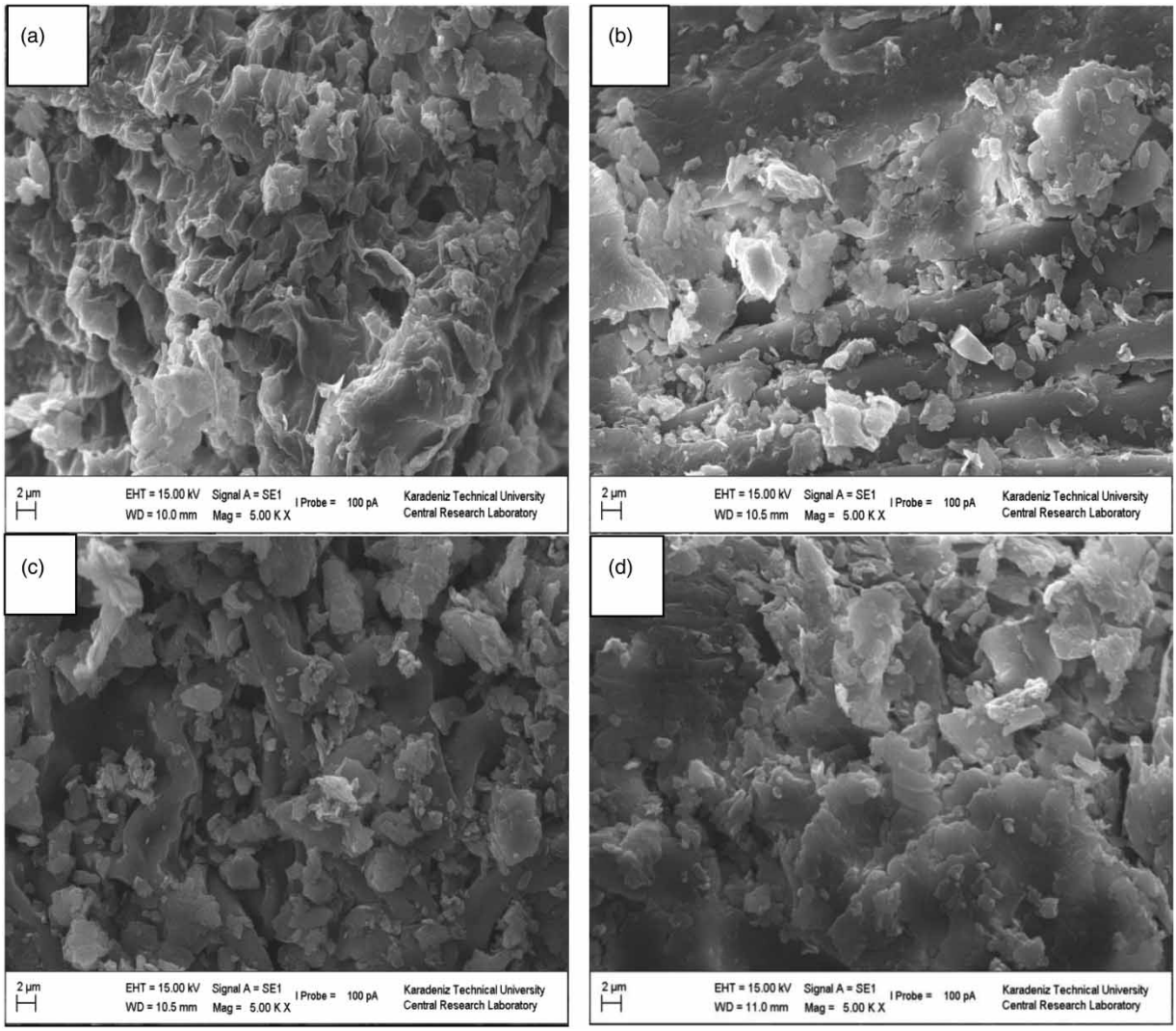


**Figure 2** | SEM micrographs of (a) NML; (b) AAM; (c) CAM; and (d) OAM.

Equilibrium time was optimized as 60 min for MO adsorption onto MPC (Siraorarnroj *et al.* 2022), and as 35 min for MB adsorption with biochar obtained from mulberry leaves (Khan & Farooqui 2022).

The pseudo-first order (PFO), pseudo-second order (PSO), and intra-particle diffusion (IPD) models were applied to the experimental data to determine the adsorption rate and to explain the adsorption mechanism of RBBR on AAM, CAM, and OAM. The linear rate equations for PFO (Lagergren 1898), PSO (Ho & McKay 1998) and IPD (Weber Jr & Morriss 1963) models are presented in Equations (2), (3), and (4), respectively:

$$\ln(q_e - q_t) = \ln q_e - k_1 t \tag{2}$$

$$\frac{t}{q_t} = \frac{1}{k_2 q_e^2} + \frac{t}{q_e} \tag{3}$$

$$q_t = k_{id} t^{1/2} + c \tag{4}$$

where $q_e$ (mg g$^{-1}$) and $q_t$ (mg g$^{-1}$) are the amounts of the RBBR adsorbed on AAM, CAM and OAM at equilibrium and at any time $t$ (min), respectively. $k_1$ (min$^{-1}$), $k_2$ (g mg$^{-1}$min$^{-1}$), and $k_{id}$ (mg g$^{-1}$min$^{-1/2}$) are the rate constants of the PFO, PSO, and IPD models, respectively. The magnitude of $C$ provides some indication about the thickness of the boundary layer. According

Downloaded from http://iwaponline.com/jwh/article-pdf/21/7/869/1263352/jwh0210869.pdf
by guest

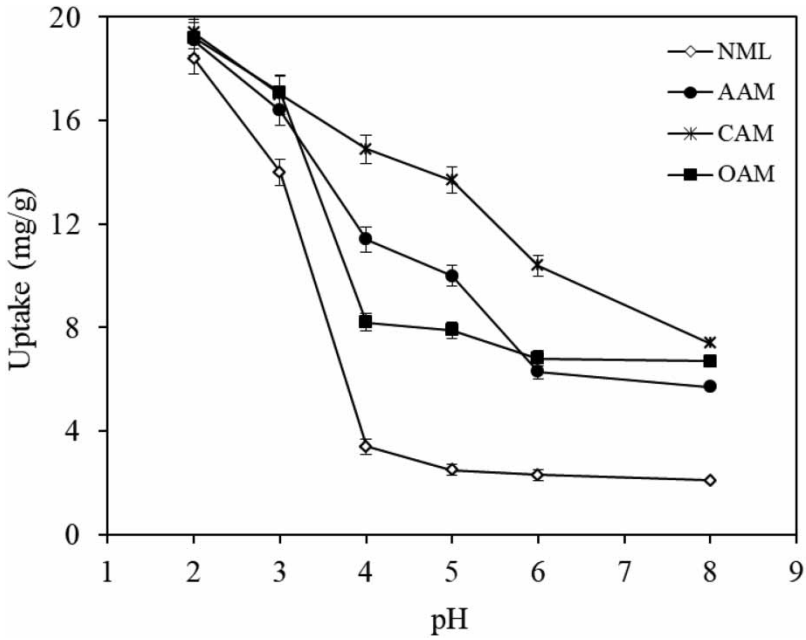


**Figure 3** | Influences of initial pH on RBBR uptake.

to the PFO model, $k_1$ and $q_e$ values are acquired from the slope and intercept of the plot of $\ln(q_e–q_t)$ versus $t$, respectively. Considering the PSO model, $q_e$ and $k_2$ values are calculated from the slope and intercept of the figure drawn between $t/q_t$–$t$, respectively (Supplementary material, Figure S3). On the other hand, IPD model parameters $k_{id}$ and $C$ are observed from the slope and intercept of the plot of $q_t$ versus $t^{1/2}$, respectively. The resulting constants for each model are revealed in Table 1, along with the related correlation coefficients ($R^2$).

**Table 1** | Kinetic model parameters for RBBR adsorption

| | **Type of adsorbent** | | |
|---|---|---|---|
| | **AAM** | **CAM** | **OAM** |
| $q_{e,\exp}$ | 19.4 | 19.2 | 19.6 |
| PFO | | | |
| $k_1$ | −0.014 | −0.014 | −0.018 |
| $q_{e,\mathrm{cal}}$ | 12.3 | 9.73 | 10.1 |
| $R^2$ | 0.940 | 0.940 | 0.958 |
| PSO | | | |
| $k_2$ | 0.00302 | 0.00483 | 0.00502 |
| $q_{e,\mathrm{cal}}$ | 20.1 | 19.6 | 20.0 |
| $R^2$ | 0.999 | 0.999 | 0.999 |
| IPD | | | |
| $k_{id,1}$ | 2.24 | 2.76 | 2.77 |
| $R^2$ | 0.966 | 0.999 | 0.994 |
| $k_{id,2}$ | 0.97 | 0.46 | 0.79 |
| $R^2$ | 0.999 | 0.964 | 0.981 |
| $C$ | 5.53 | 7.31 | 7.23 |

Downloaded from http://iwaponline.com/jwh/article-pdf/21/7/869/1263352/jwh0210869.pdf
by guest

The $q_{e,\text{exp}}$ values for AAM, CAM, and OAM were calculated as 19.4, 19.2, and 19.6 mg $g^{-1}$, respectively. As a result of applying the PFO model to the experimental data, $q_{e,\text{cal}}$ values for AAM, CAM, and OAM were found to be 12.3, 9.73, and 10.1 mg $g^{-1}$ and $R^2$ values were 0.940, 0.940, and 0.958, respectively. By the application PSO model, $q_{e,\text{cal}}$ values were found to be 20.1, 19.6, and 20.0 mg $g^{-1}$ for AAM, CAM, and OAM, respectively, and $R^2$ values are higher than 0.999 for all three adsorbents (Supplementary material, Figure S3). Considering these data, it is noticed that the PSO model is dominant in the adsorption mechanism of RBBR onto AAM, CAM, and OAM because of the proximity of the $q_e$ values computed experimentally with the $q_e$ values observed by the application of the model. On the other hand, the higher $R^2$ values were achieved by the PSO model. This suggests that chemisorption is effective in the adsorption mechanism (Amiri *et al.* 2019). Similar results were obtained by İnal & Erduran (2015) for the adsorption of RBBR on a different type of hydrogel bead and by Zhong *et al.* (2012) for the application of activated carbon prepared by microwave assisted $H_3PO_4$ activation of peanut hull in RBBR removal. In addition to these observations, according to the IPD model, a noticeable multilinear plot ($q_t$ versus $t^{1/2}$) demonstrates that the adsorption process occurs in three main steps. The first step is explained by film diffusion, which corresponds to the transport of dye molecules from the bulk solution to the external surface of the adsorbent. The second step controls the adsorption rate by pore diffusion (intraparticle diffusion) which is attributed to a gradual adsorption occurring from the external surface into the pores of the adsorbent. The third step is explained by the rapid adsorption of dye molecules onto the active sites of the pores' internal surfaces and does not generally determine the adsorption rate (Wang *et al.* 2005; Hameed & El-Khaiary 2008). In order to decide which of these stages is dominant in the RBBR adsorption mechanism, the rate constant is calculated for each stage. It is known that the stage with the smallest rate constant value is effective on the mechanism. The rate constant ($k_{id}$) values calculated for each stage are given in Table 1. Since the final stage, which is the equilibrium state, occurs very quickly, the rate constant has high values. Therefore, the effect of this step on the mechanism is neglected. It is seen that the rate constant values obtained from the intraparticle diffusion stage for all three adsorbents are lower than the rate constant values calculated from the film diffusion stage (Table 1). Therefore, it is thought that intraparticle diffusion is effective in the adsorption mechanism of RBBR. However, another parameter to be considered at this point is the $C$ constant. The calculated $C$ constant is nonzero for all adsorbents. Therefore, it can be concluded that film diffusion and intraparticle diffusion are effective together in the adsorption of RBBR on AAM, CAM, and OAM (Bensalah *et al.* 2017).

### 3.4. Influences of initial dye concentration on RBBR uptake and evaluation of adsorption isotherms

In order to assess the impact of initial dyestuff concentration on the adsorption efficiency of RBBR on NML, AAM, CAM, and OAM and also to obtain the adsorption isotherm data, the RBBR solutions with initial concentrations of 50–1,000 mg $L^{-1}$ were treated separately with 5.0 g $L^{-1}$ of adsorbent for 240 min of contact time. Results of the experimental studies indicated that as the RBBR concentration is increased from 50 to 1,000 mg $L^{-1}$, the uptake amount increases from 9.77, 9.46, 9.67, and 9.90 mg $g^{-1}$ to 64.8, 91.5, 82.8, and 92.2 mg $g^{-1}$ for NML, AAM, CAM, and OAM, respectively (Figure 4). The increase in RBBR concentration at constant adsorbent amounts causes a concentration gradient, a driving force for adsorption, and

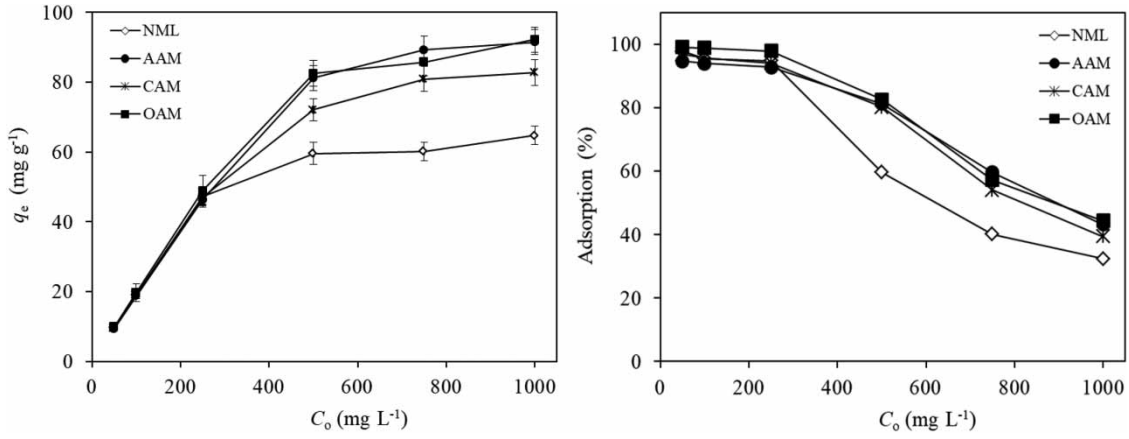


**Figure 4** | Impact of initial RBBR concentration on its retention.

Downloaded from http://iwaponline.com/jwh/article-pdf/21/7/869/1263352/jwh0210869.pdf
by guest

hence the RBBR adsorption amount onto per gram of adsorbent ($q_e$) increases. On the contrary, at high RBBR levels, the percentage of adsorption is expected to decrease due to over-saturated active adsorption surfaces on the adsorbent (Sharma *et al.* 2010). Namely, as RBBR concentration is increased from 50 to 1,000 mg $L^{-1}$, the removal percentages decrease from 97.7, 94.6, 96.7, and 99.8% to 32.4, 43.2, 39.4, and 44.3% for NML, AAM, CAM and OAM, respectively (Figure 4).

Interactions between the adsorbent and adsorbate can be interpreted by some useful data attained from the adsorption isotherms. Langmuir, Freundlich, and Dubinin–Radushkevich (D–R) isotherm models were utilized for describing the characteristics of RBBR adsorption onto NML, AAM, CAM, and OAM at equilibrium conditions. In the adsorption process, specific homogeneous sites play the role of monolayers which prevents the interactions between the adsorbed species and is the characteristic of Langmuir model (Langmuir 1918). On the other hand, according to the Freundlich model, heterogeneous surfaces which have different energy are available on the adsorbent for multilayer adsorption (Freundlich 1906). The D–R model also provides extra information about the type of adsorption (Dubinin & Radushkevich 1947).

Langmuir model in linear form (Equation (5)) includes $q_e$ (mg $g^{-1}$); the amount of RBBR adsorbed per unit adsorbent mass, $C_e$ (mg $L^{-1}$); the level of RBBR at equilibrium, $b$ (L $mg^{-1}$); free energy of the adsorption, and $q_{max}$ (mg $g^{-1}$); adsorption capacity. Herein, the intercept and the slope of $C_e/q_e$ versus $C_e$ plot were used to obtain $b$ and $q_{max}$, respectively:

$$\frac{C_e}{q_e} = \frac{C_e}{q_{max}} + \frac{1}{bq_{max}} \tag{5}$$

The feasibility of an adsorption process is estimated by evaluating the non-dimensional parameter $R_L$, which is calculated with the aid of Equation (6). $R_L$ values between 0 and 1 reveal favorable adsorption (Senturk *et al.* 2010). Here, $C_0$ (mg $L^{-1}$) is the initial concentration of adsorbate and $b$ (L $mg^{-1}$) is the Langmuir constant:

$$R_L = \frac{1}{1 + b.C_o} \tag{6}$$

The linear form of the Freundlich isotherm model is expressed by Equation (7):

$$\ln q_e = \ln K_f + \frac{1}{n} \ln C_e \tag{7}$$

where $K_f$ (mg $g^{-1}$); indicate the adsorption capacity, $n$; a unitless constant representing the adsorption density. To obtain the numerical values of $K_f$ and $n$, $\ln q_e$ versus $\ln C_e$ a graph is plotted and the constants, $n$ and $K_f$, are obtained from the slope and intercept of this graph, respectively. The fact that the $n$ constant is in the range of 1–10 indicates the suitability of the developed process. Further information on the adsorption mechanism of RBBR is available from D–R model presented in Equation (8):

$$\ln q_e = \ln q_m - \beta\varepsilon^2 \tag{8}$$

$$\varepsilon = RT \ln\left(1 + \frac{1}{C_e}\right) \tag{9}$$

$$E = \left(\frac{1}{-2\beta}\right)^{1/2} \tag{10}$$

where $q_e$ is the amount of RBBR adsorbed onto per unit mass of adsorbent (mol $g^{-1}$), $q_m$ is the monolayer adsorption capacity (mol $g^{-1}$), $b$ is the activity coefficient related to the mean adsorption energy (kJ$^2$ $mol^{-2}$), $\varepsilon$ is the Polanyi potential and $C_e$ is the equilibrium RBBR concentration (mol $L^{-1}$) in aqueous solution. $q_m$ and $\beta$ are the D–R model constants, observed from the intercept and the slope of the linear plot of $\ln q_e$ versus $\varepsilon^2$, respectively. Mean adsorption energy, $E$ (kJ $mol^{-1}$), which provides an idea about the adsorption mechanism, can be obtained by using Equation (10). Namely, the $E$ value being in the range of 8–16 kJ $mol^{-1}$ indicates that the adsorption process mainly proceeds through the ion exchange mechanism. The $E$ value

Downloaded from http://iwaponline.com/jwh/article-pdf/21/7/869/1263352/jwh0210869.pdf
by guest

lower than 8 kJ $mol^{-1}$ indicates physical adsorption, while a value greater than 16 kJ $mol^{-1}$ demonstrates that chemical adsorption has occurred (Helfferich 1962; Mosai *et al.* 2020).

Figure 5 provides a comparison of equilibrium isotherms between experimental and theoretical data. The fact that the $R^2$ values based on the Langmuir model for both natural and modified adsorbents are higher than the Freundlich model indicates that RBBR adsorption occurs in the form of a monolayer on the homogeneous adsorbent surface. Similar results were also obtained in the MO adsorption process on the MPC surface (Siraorarnroj *et al.* 2022). The RBBR adsorption capacity of NML, AAM, CAM, and OAM was achieved as 64.5, 95.2, 84.8, and 91.7 mg $g^{-1}$, respectively, using the Langmuir equation (Table 2). These results demonstrated that the modification with carboxylic acid significantly increases the anionic dyestuff adsorption capacity of mulberry leaves. The adsorption capacity of the proposed adsorbents is superior to that of most of the other difficult-to-prepare and costly sorbents listed in Table 3 (Iqbal & Saeed 2007; Ada *et al.* 2009; İnal & Erduran 2015; Li *et al.* 2015; Chinoune *et al.* 2016; Abbasi 2017; Saputra *et al.* 2017; Mate & Mishra 2020). Apart from these adsorbents, the MO and MB adsorption capacities of mulberry leaves modified with different methods were determined as 0.0181 mg $g^{-1}$ (Siraorarnroj *et al.* 2022) and 6.55 mg $g^{-1}$ (Khan & Farooqui 2022), respectively. Between 50 and 1,000 mg $L^{-1}$ initial RBBR concentrations, the $R_L$ values were in the range of 0.180–0.011 for NML, 0.294–0.020 for AAM, 0.217–0.014 for CAM and 0.130–0.007 for OAM, demonstrating the suitability of the developed adsorption method. The fact that the $n$ values obtained from the Freundlich model fall within the range of 1–10 also confirms the suitability of RBBR retention on adsorbents (Le *et al.* 2019). The $E$ values calculated using the D–R model were in the range of 8–16 kJ $mol^{-1}$ in all cases, pointing out that the adsorption mechanisms of RBBR probably occur via the ion exchange mechanism (Thamilarasi *et al.* 2018).

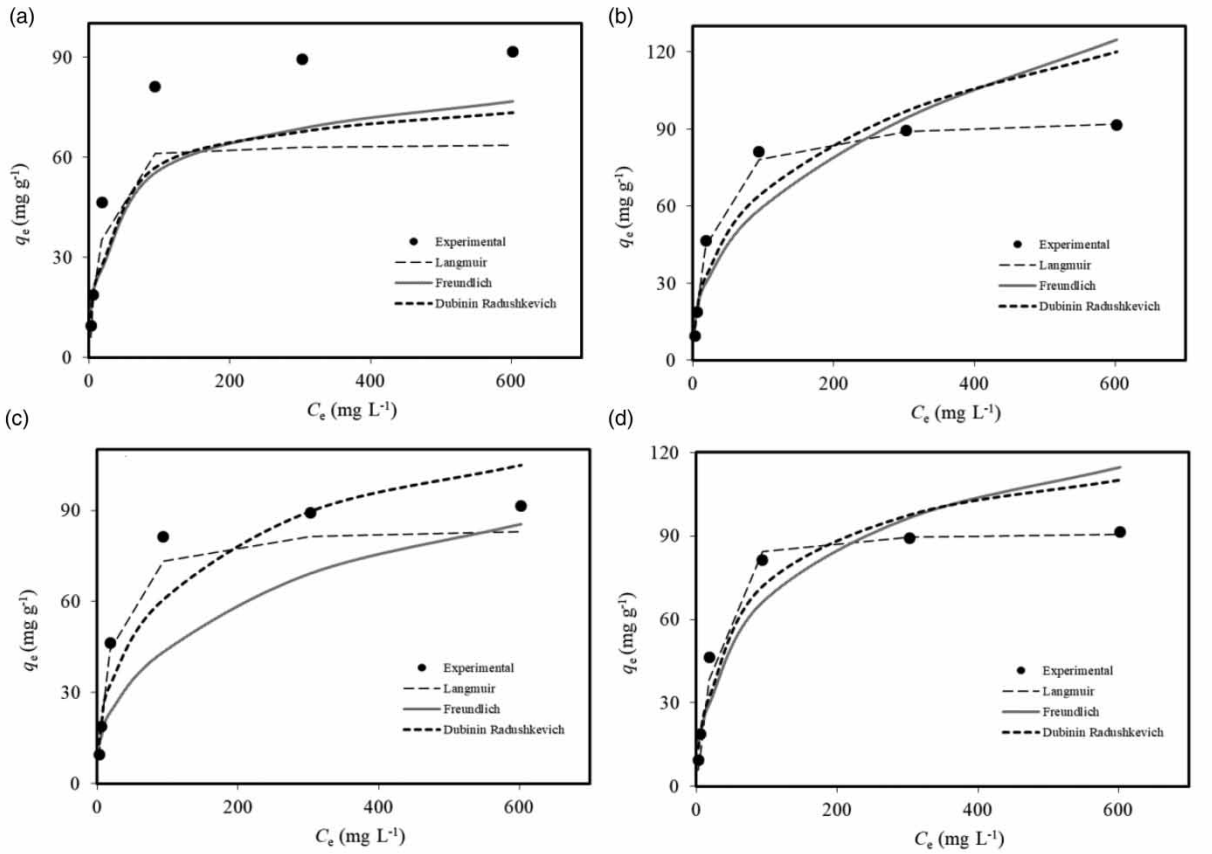


**Figure 5** | Comparison of equilibrium isotherms between the experimental data and theoretical data for (a) NML; (b) AAM; (c) CAM; and (d) OAM.

Downloaded from http://iwaponline.com/jwh/article-pdf/21/7/869/1263352/jwh0210869.pdf
by guest

**Table 2** | Isotherm parameters for RBBR adsorption

| | Type of adsorbent | | | |
|---|---|---|---|---|
| | **NML** | **AAM** | **CAM** | **OAM** |
| Langmuir isotherm | | | | |
| $q_{max}$ | 64.5 | 95.2 | 84.8 | 91.7 |
| $B$ | 0.091 | 0.048 | 0.072 | 0.134 |
| $R^2$ | 0.998 | 0.999 | 0.999 | 0.999 |
| Freundlich isotherm | | | | |
| $K_f$ | 13.2 | 9.16 | 11.6 | 18.1 |
| $n$ | 3.71 | 2.45 | 2.89 | 3.44 |
| $R^2$ | 0.834 | 0.880 | 0.876 | 0.875 |
| D–R isotherm | | | | |
| $q_m$ | 11.9 | 18.4 | 15.6 | 14.8 |
| $\beta$ | − 0.0023 | −0.0035 | −0.0029 | −0.0023 |
| $E$ | 14.7 | 12.0 | 13.1 | 14.7 |
| $R^2$ | 0.879 | 0.922 | 0.921 | 0.919 |

### 3.5. Influences of adsorbent concentration on RBBR removal

The influences of AAM, CAM, and OAM amount on RBBR removal from aqueous media were assessed between 1.0 and 20.0 g $L^{-1}$ of adsorbent amount, in the experimental conditions of 240 min of equilibrium time and initial solution pH of 2.0 for 200 mg $L^{-1}$ of initial RBBR concentration. The amount of RBBR adsorption at equilibrium and RBBR removal percentages (Figure 6) plotted against the AAM, CAM, and OAM amounts. The increase in the amount of adsorbent at constant RBBR concentration causes the formation of unsaturated adsorption surfaces and agglomeration of the adsorbent (Crini *et al.* 2007). Therefore the amount of adsorbed RBBR per gram of adsorbent decreased from 97.1, 101.6 and 102.9 mg $g^{-1}$ to 9.79, 9.80, and 9.85 mg $g^{-1}$ for AAM, CAM, and OAM respectively. However, the adsorption percentage increased from 48.6, 50.8, and 51.4% to 97.9, 98.0, and 98.5% for AAM, CAM, and OAM, respectively as increasing in the amount of adsorbent which lead to an increase in the active adsorption sites (Figure 6).

**Table 3** | Comparison of the maximum RBBR adsorption capacities of various adsorbents

| **Adsorbent** | **$Q_{max}$ (mg/g)** | **Reference** |
|---|---|---|
| ZnO fine powder (Z300) | 89.3 | Ada *et al.* (2009) |
| ZnO fine powder (Z075) | 38.9 | Ada *et al.* (2009) |
| Sodium alginate/poly(N-vinyl-2-pyrrolidone) | 55.3 | İnal & Erduran (2015) |
| Bentonite coated with Mg(OH) | 66.9 | Chinoune *et al.* (2016) |
| Amino-functionalized organosilane | 21.3 | Saputra *et al.* (2017) |
| Borax cross-linked Jhingan gum hydrogel | 9.88 | Mate & Mishra (2020) |
| Porous Polyurea | 78 | Li *et al.* (2015) |
| Loofa sponge-immobilized fungal biomass | 98.8 | Iqbal & Saeed (2007) |
| Magnetic nanocomposite of chitosan/$SiO_2$/carbon nanotubes | 97.1 | Abbasi (2017) |
| NML (natural mulberry leaves) | 64.5 | This study |
| AAM (acetic acid-modified mulberry leaves) | 95.2 | |
| CAM (citric acid-modified mulberry leaves) | 84.8 | |
| OAM (oxalic acid-modified mulberry leaves) | 91.7 | |

Downloaded from http://iwaponline.com/jwh/article-pdf/21/7/869/1263352/jwh0210869.pdf
by guest

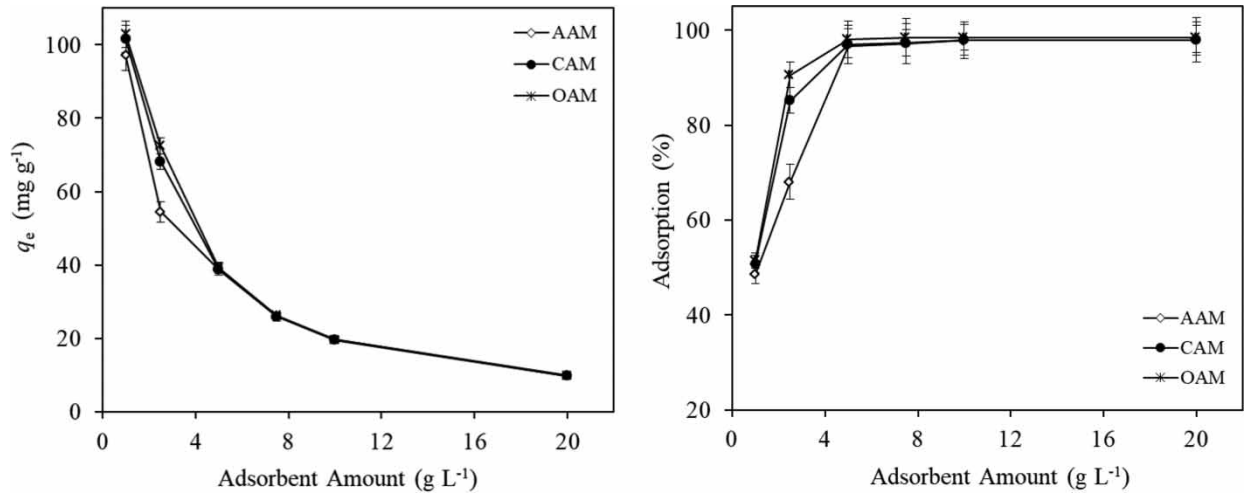


**Figure 6** | Effect of adsorbent amount on RBBR adsorption.

### 3.6. ANN modeling of the adsorption process of RBBR

The ANN model was applied to generate a prediction model for the adsorption efficiency of RBBR onto AAM, CAM, and OAM by dividing 27 experimental data randomly into three subgroups including training (70%), validation (15%), and testing (15%). Then, three-layer BP neural network model with tansig in the hidden layer and purelin in the output layer was assessed by various neuron numbers. The best performance was acquired when eight neurons were present in the hidden layer. Thereafter to achieve the best possible weights, errors, and correlations various training studies were performed. The ANN regression plot for training, validation, testing and the overall prediction set in the form of network output versus adsorption efficiency is given in Figure 7(a)–7(c) for AAM, CAM, and OAM, respectively. Based on the regression analysis, it is seen that the network output values are close to the experimental adsorption efficiency in all cases. The overall prediction set was obtained as 0.998, 0.994 and 0.999 for AAM, CAM, and OAM, respectively. The results demonstrated that the ANN model is suitable for the prediction of RBBR adsorption efficiency with sensible accuracy.

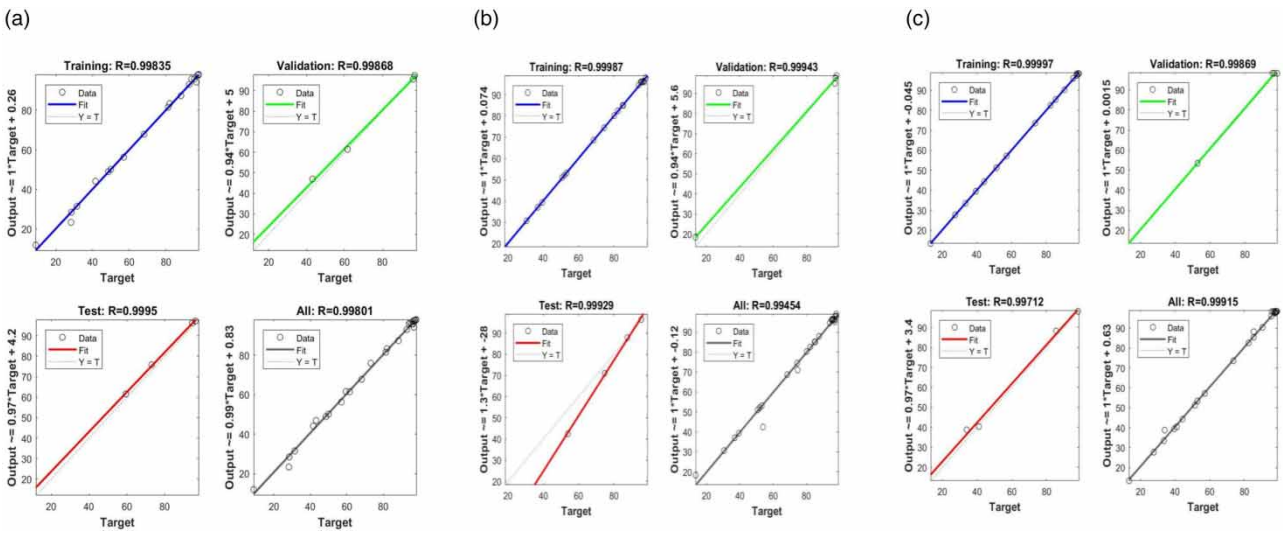


**Figure 7** | Outcomes of ANN algorithm for estimation of RBBR recovery percentage of (a) AAM; (b) CAM; and (c) OAM.

Downloaded from http://iwaponline.com/jwh/article-pdf/21/7/869/1263352/jwh0210869.pdf
by guest

## 4. CONCLUSION

In the present research, the removal of an anionic dye, RBBR, from aqueous media by NML and AAM, OAM, and CAM mulberry leaves via an adsorption process was studied for the first time. This study gets attention from the environmental and industrial perspectives since there is a great need to uptake the harmful RBBR dye by cost-effective and abundant materials from wastewater before the discharge step. The influences of various experimental factors on the adsorption efficiency were investigated. The optimum initial solution pH was determined as 2.0 for RBBR adsorption. It was observed that the adsorption efficiency reached its maximum after 240 min of equilibrium time. RBBR adsorption capacity of carboxylic acid modified adsorbents was also found to be higher than many other adsorbents mentioned in the literature. The results of this study demonstrated that the modification of mulberry leaves with different types of carboxylic acids enhances the adsorption efficiency of anionic dyes and suggests a low-cost and easily available adsorbent for the uptake of harmful RBBR dye from aqueous solutions. In the future, considering the experimental parameters optimized by using aqueous solutions in the laboratory environment, an application will be carried out directly on textile wastewater in order to remove both anionic and cationic dyes. In addition, the usability of the developed adsorbents in the removal of various heavy metal ions from wastewater will also be tested.

## FUNDING

The financial support from the Unit of the Scientific Research Projects of Karadeniz Technical University is gratefully acknowledged.

## DATA AVAILABILITY STATEMENT

All relevant data are included in the paper or its Supplementary Information.

## REFERENCES

Abbasi, M. 2017 Synthesis and characterization of magnetic nanocomposite of chitosan/$SiO_2$/carbon nanotubes and its application for dyes removal. *Journal of Cleaner Production* **145**, 105–113.

Ada, K., Ergene, A., Tan, S. & Yalcın, E. 2009 Adsorption of Remazol Brilliant Blue R using ZnO fine powder: Equilibrium, kinetic and thermodynamic modeling studies. *Journal of Hazardous Materials* **165** (1–3), 637–644.

Ahmad, M. A., Puad, N. A. A. & Bello, O. S. 2014 Kinetic, equilibrium and thermodynamic studies of synthetic dye removal using pomegranate peel activated carbon prepared by microwave-induced KOH activation. *Water Resources and Industry* **6**, 18–35.

Ali, H. 2010 Biodegradation of synthetic dyes – A review. *Water, Air, & Soil Pollution* **213**, 251–273.

Amiri, M. J., Bahrami, M. & Dehkhodaie, F. 2019 Optimization of Hg(II) adsorption on bio-apatite based materials using CCD-RSM design: Characterization and mechanism studies. *Journal of Water and Health* **17** (4), 556–567.

Bensalah, H., Bekheet, M. F., Younssi, S. A., Ouammou, M. & Gurlo, A. 2017 Removal of cationic and anionic textile dyes with Moroccan natural phosphate. *Journal of Environmental Chemical Engineering* **5** (3), 2189–2199.

Chinoune, K., Bentaleb, K., Bouberka, Z., Nadim, A. & Maschke, U. 2016 Adsorption of reactive dyes from aqueous solution by dirty bentonite. *Applied Clay Science* **123**, 64–75.

Chumpiboon, A., Thongsubsai, K., Pongsiri, T., Knijnenburg, J. T. N. & Ngernyen, Y. 2022 Removal of cationic dye from textile wastewater using treated bagasse fly ash: An industrial waste. *Engineering and Applied Science Research* **49** (3), 381–394.

Crini, G., Peindy, H. N., Gimbert, F. & Robert, C. 2007 Removal of C.I. Basic Green 4 (Malachite Green) from aqueous solutions by adsorption using cyclodextrin-based adsorbent: Kinetic and equilibrium studies. *Separation and Purification Technology* **53** (1), 97–110.

Dubinin, M. M. & Radushkevich, L. V. 1947 Equation of the characteristic curve of activated charcoal. *Proceedings of the Academy of Sciences of the USSR, Physical Chemistry Section* **55**, 331–333.

Duran, C., Ozdes, D., Gundogdu, A. & Senturk, H. B. 2011 Kinetics and isotherm analysis of basic dyes adsorption onto almond shell (*Prunus dulcis*) as a low cost adsorbent. *Journal of Chemical & Engineering Data* **56** (5), 2136–2147.

Ewuzie, U., Saliu, O. D., Dulta, K., Ogunniyi, S., Bajeh, A. O., Iwuozori, K. O. & Ighalo, J. O. 2022 A review on treatment technologies for printing and dyeing wastewater (PDW). *Journal of Water Process Engineering* **50**, 103273.

Freundlich, H. M. F. 1906 Uber die adsorption in Losungen. *Zeitschrift für Physikalische Chemie* **57**, 385–470.

Ghadirimoghaddam, D., Gheibi, M. & Eftekhari, M. 2021 Graphene oxide-cyanuric acid nanocomposite as a novel adsorbent for highly efficient solid phase extraction of $Pb^{2+}$ followed by electrothermal atomic absorption spectrometry; statistical, soft computing and mechanistic efforts. *International Journal of Environmental Analytical Chemistry* https://doi.org/10.1080/03067319.2020.1861260.

Guo, X., Liu, Z., Tong, Z., Jiang, N. & Chen, W. 2022 Adsorption of Rhodamine B from an aqueous solution by acrylic-acid-modified walnut shells: characterization, kinetics, and thermodynamics. *Environmental Technology* https://doi.org/10.1080/09593330.2021.2011430.

Downloaded from http://iwaponline.com/jwh/article-pdf/21/7/869/1263352/jwh0210869.pdf
by guest

Hameed, B. H. & El-Khaiary, M. I. 2008 Kinetics and equilibrium studies of malachite green adsorption on rice straw-derived char. *Journal of Hazardous Materials* **153** (1–2), 701–708.

Helfferich, F. 1962 *Ion Exchange*. McGraw-Hill, New York.

Herkommerová, K., Dostál, J. & Pichová, I. 2018 Decolorization and detoxification of textile wastewaters by recombinant *Myceliophthora thermophila* and *Trametes trogii* laccases. *Biotech* **8**, 505.

Ho, Y. S. & McKay, G. 1998 Kinetic models for the sorption of dye from aqueous solution by wood. *Process Safety and Environmental Protection* **76** (2), 183–191.

Hong, G.-B. & Wang, Y.-K. 2017 Synthesis of low-cost adsorbent from rice bran for the removal of reactive dye based on the response surface methodology. *Applied Surface Science* **423**, 800–809.

İnal, M. & Erduran, N. 2015 Removal of various anionic dyes using sodium alginate/poly(N-vinyl-2-pyrrolidone) blend hydrogel beads. *Polymer Bulletin* **72**, 1735–1752.

Iqbal, M. & Saeed, A. 2007 Biosorption of reactive dye by loofa sponge-immobilized fungal biomass of *Phanerochaete chrysosporium*. *Process Biochemistry* **42** (7), 1160–1164.

Jawad, A. H., Abdulhameed, A. S., Kashi, E., Yaseen, Z. M., ALOthman, Z. A. & Khan, M. R. 2022 Cross-linked chitosan-glyoxal/kaolin clay composite: Parametric optimization for color removal and COD reduction of remazol brilliant blue R Dye. *Journal of Polymers and the Environment* **30**, 164–178.

Karadeniz, M. & Osma, E. 2019 Determination of heavy metal accumulation in mulberries (*Morus alba* L.) growing in malatya. *Erzincan University Journal of Science and Technology* **12** (2), 893–901.

Khajeh, M., Moosavi-Movahedi, A. A., Shakeri, M., Zadeh, F. M., Khajeh, A. & Bohlooli, M. 2015 Dispersive solid phase extraction combined with dispersive liquid–liquid extraction for the determination of BTEX in soil samples: ant colony optimization–artificial neural network. *Journal of Chemometrics* **29** (4), 245–252.

Khan, F. A. & Farooqui, M. 2022 Removal of methylene blue dye from aqueous solutions onto *Morus nigra* L. (mulberry tree) leaves powder and its biochar– equilibrium, kinetic and thermodynamic study. *International Journal of Environmental Analytical Chemistry* https://doi.org/10.1080/03067319.2022.2103691.

Lagergren, S. 1898 About the theory of so-called adsorption of soluble substance, Kungliga Svenska Vetenskapsakademiens. *Handlingar* **24**, 1–39.

Langmuir, I. 1918 The adsorption of gases on plane surfaces of glass, mica and platinum. *Journal of American Chemical Society* **40** (9), 1361–1403.

Le, V. T., Tran, T. K. N., Tran, D. L., Le, H. S., Doan, V. D., Bui, Q. D. & Nguyen, H. T. 2019 One-pot synthesis of a novel magnetic activated carbon/clay composite for removal of heavy metals from aqueous solution. *Journal of Dispersion Science and Technology* **40** (12), 1761–1776.

Li, S., Han, H., Zhu, X., Jiang, X. & Kong, X. Z. 2015 Preparation and formation mechanism of porous polyurea by reaction of toluene diisocyanate with water and Its application as adsorbent for anionic dye removal. *Chinese Journal of Polymer Science* **33**, 1196–1210.

Liu, X., Huang, L., Wang, L., Wang, C., Wu, X., Dong, G. & Liu, Y. 2018 Preparation, adsorptive properties and chemical regeneration studies of high-porous activated carbon derived from *Platanus orientalis* leaves for Cr(VI) removal. *Journal of Water and Health* **16** (5), 814–826.

Ma, C. M., Hong, G. B. & Wang, Y. K. 2020 Performance evaluation and optimization of dyes removal using rice bran-Based magnetic composite adsorbent. *Materials* **13** (12), 2764.

Malook, K. & Khan, H. 2020 Removal of Cd(II) from water using zero valent iron/copper functionalized spent tea. *Water Science and Technology* **82** (11), 2552–2561.

Mate, C. J. & Mishra, S. 2020 Synthesis of borax cross-linked Jhingan gum hydrogel for remediation of Remazol Brilliant Blue R (RBBR) dye from water: Adsorption isotherm, kinetic, thermodynamic and biodegradation studies. *International Journal of Biological Macromolecules* **151**, 677–690.

Mechichi, T., Mhiri, N. & Sayadi, S. 2006 Remazol Brilliant Blue R decolourization by the laccase from *Trametes trogii*. *Chemosphere* **64** (6), 998–1005.

Miyah, Y., Benjelloun, M., Lahrichi, A., Mejbar, F., Iaich, S., El Mouhri, G., Kachkoul, R. & Zerrouq, F. 2021 Highly-efficient treated oil shale ash adsorbent for toxic dyes removal: Kinetics, isotherms, regeneration, cost analysis and optimization by experimental design. *Journal of Environmental Chemical Engineering* **9** (6), 106694.

Moharami, S. & Jalali, M. 2013 Removal of phosphorus from aqueous solution by Iranian natural adsorbents. *Chemical Engineering Journal* **223**, 328–339.

Mosai, A. K., Chimuka, L., Cukrowska, E. M., Kotze, I. A. & Tutu, H. 2020 Removal of platinum (IV) from aqueous solutions with yeast-functionalized bentonite. *Chemosphere* **239**, 124768.

Nayak, A. K. & Pal, A. 2021 Enhanced adsorption of gentian violet dye from water using lignocellulosic agricultural waste modified with di- and tri-carboxylic acids: Artificial intelligence modeling, practical comprehension, mechanistic and regeneration analyses. *Journal of Environmental Chemical Engineering* **9** (4), 105578.

Ozdes, D., Duran, C., Senturk, H. B., Avan, H. & Bicer, B. 2014 Kinetics, thermodynamics, and equilibrium evaluation of adsorptive removal of methylene blue onto natural illitic clay mineral. *Desalination and Water Treatment* **52** (1–3), 208–218.

Downloaded from http://iwaponline.com/jwh/article-pdf/21/7/869/1263352/jwh0210869.pdf
by guest

Ozdes, D., Gundogdu, A., Duran, C. & Senturk, H. B. 2010 Evaluation of adsorption characteristics of malachite green onto almond shell (*Prunus dulcis*). *Separation Science and Technology* **45**, 2076–2085.

Reghioua, A., Barkat, D., Jawad, A. H., Abdulhameed, A. S., Al-Kahtani, A. A. & ALOthman, Z. A. 2021 Parametric optimization by Box–Behnken design for synthesis of magnetic chitosan-benzil/ZnO/$Fe_3O_4$ nanocomposite and textile dye removal. *Journal of Environmental Chemical Engineering* **9** (3), 105166.

Saputra, O. A., Rachma, A. H. & Handayani, D. S. 2017 Adsorption of remazol brilliant blue R using amino-functionalized organosilane in aqueous solution. *Indonesian Journal of Chemistry* **17** (3), 343–350.

Senturk, H. B., Ozdes, D. & Duran, C. 2010 Biosorption of Rhodamine 6G from aqueous solutions onto almond shell (*Prunus dulcis*) as a low cost biosorbent. *Desalination* **252** (1–3), 81–87.

Sharma, P., Kaur, R., Baskar, C. & Chung, W.-J. 2010 Removal of methylene blue from aqueous waste using rice husk and rice husk ash. *Desalination* **259** (1–3), 249–257.

Shojaei, S., Rahmani, M., Khajeh, M. & Abbasian, A. R. 2021 Magnetic-nanoparticle-based dispersive micro-solid phase extraction for the determination of crystal violet in environmental water samples. *ChemistrySelect* **6** (19), 4782–4790.

Siraorarnroj, S., Kaewtrakulchai, N., Fuji, M. & Eiad-ua, A. 2022 High performance nanoporous carbon from mulberry leaves (*Morus alba* L.) residues via microwave treatment assisted hydrothermal-carbonization for methyl orange adsorption: kinetic, equilibrium and thermodynamic studies. *Materialia* **21**, 101288.

Thamilarasi, M. J. V., Anilkumar, P., Theivarasu, C. & Sureshkumar, M. V. 2018 Removal of vanadium from wastewater using surface-modified lignocellulosic material. *Environmental Science and Pollution Research* **25** (26), 26182–26191.

Tian, A., Xiaojun, J. & Qingyu, L. 2020 Novel adsorbents based upon carboxylic acid-modified *Phyllostachys pubescens* powder: preparation, characterization and application for adsorbing lead(II) from aqueous solution. *Separation Science and Technology* **55** (7), 1249–1259.

Vakili, M., Rafatullah, M., Salamatinia, B., Abdullah, A. Z., Ibrahim, M. H., Tan, K. B., Gholami, Z. & Amouzgar, P. 2014 Application of chitosan and its derivatives as adsorbents for dye removal from water and wastewater: A review. *Carbohydrate Polymers* **113**, 115–130.

Vijayaraghavan, K. & Yun, Y. S. 2008 Biosorption of C.I. reactive black 5 from aqueous solution using acid treated biomass of brown seaweed *Laminaria* sp. *Dyes and Pigments* **76** (3), 726–732.

Wang, S., Li, L., Wu, H. & Zhu, Z. H. 2005 Unburned carbon as a low-cost adsorbent for treatment of methylene blue-containing wastewater. *Journal of Colloid and Interface Science* **292** (2), 336–343.

Wang, S., Soudi, M., Li, L. & Zhu, Z. H. 2006 Coal ash conversion into effective adsorbents for removal of heavy metals and dyes from wastewater. *Journal of Hazardous Materials* **133** (1–3), 243–251.

Weber Jr, W. J. & Morriss, J. C. 1963 Kinetics of adsorption on carbon from solution. *Journal of the Sanitary Engineering Division* **89**, 31–60.

Zhang, H., Xing, L., Liang, H., Ren, J., Ding, W., Wang, Q., Geng, Z. & Xu, C. 2022 Efficient removal of Remazol Brilliant Blue R from water by a cellulose-based activated carbon. *International Journal of Biological Macromolecules* **207**, 254–262.

Zhong, Z.-Y., Yang, Q., Li, X.-M., Luo, K., Liu, Y. & Zeng, G.-M. 2012 Preparation of peanut hull-based activated carbon by microwave-induced phosphoric acid activation and its application in Remazol Brilliant Blue R adsorption. *Industrial Crops and Products* **37** (1), 178–185.

First received 13 January 2023; accepted in revised form 7 June 2023. Available online 20 June 2023

Downloaded from http://iwaponline.com/jwh/article-pdf/21/7/869/1263352/jwh0210869.pdf
by guest